

Infrared Scattering of Cloud in an Isothermal Atmosphere

CHONGXING FAN^a AND XIANGLEI HUANG^a

^a *Department of Climate and Space Sciences and Engineering, University of Michigan, Ann Arbor, Michigan*

(Manuscript received 21 March 2023, in final form 14 August 2023, accepted 20 September 2023)

ABSTRACT: In the absence of scattering, thermal contrast in the atmosphere is the key to infrared remote sensing. Without the thermal contrast, the amount of absorption will be identical to the amount of emission, making the atmospheric vertical structure undetectable using remote sensing techniques. Here we show that, even in such an isothermal atmosphere, the scattering of clouds can cause a distinguishable change in upwelling radiance at the top of the atmosphere. A two-stream analytical solution, as well as a budget analysis based on Monte Carlo simulations, are used to offer a physical explanation of such influence on an idealized isothermal atmosphere by cloud scattering: it increases the chance of photons being absorbed by the atmosphere before they can reach the boundaries (both top and bottom), which leads to a reduction of TOA upwelling radiance. Actual sounding profiles and cloud properties inferred from satellite observations within 6-h time frames are fed into a more realistic and comprehensive radiative transfer model to show such cloud scattering effect, under nearly isothermal circumstances in the lower troposphere, can lead to $\sim 1\text{--}1.5\text{-K}$ decrease in brightness temperature for the nadir-view MODIS $8.5\text{-}\mu\text{m}$ channel. The study suggests that cloud scattering can provide signals useful for remote sensing applications even for such an isothermal environment.


KEYWORDS: Longwave radiation; Remote sensing; Clouds

1. Introduction

Since the seminal work by Kaplan (1959), thermal IR radiation has been used extensively to infer the vertical structure of atmospheric temperature and greenhouse gases (most notably, water vapor, ozone, and CO_2), as well as cloud properties such as cloud-top temperature and cloud optical depth. As far as IR cloud remote sensing is concerned, many retrieval algorithms have been implemented in actual operations, to name a few, split-window algorithms (e.g., Inoue 1985; McMillin 1975), CO_2 slicing algorithm (e.g., Smith et al. 1970; Chahine 1974; McCreese and Wilson 1976), and optimal estimation algorithms (e.g., Wang 2016a,b).

The vertical temperature gradient, i.e., thermal contrast, is the reason why such profiling capability exists in thermal IR remote sensing. In the absence of scattering, if there is no temperature gradient, the amount of radiation absorbed by a given atmospheric layer will be exactly the same as the amount of radiation emitted by the same layer. As a result, the observed radiance cannot be related to the vertical profiles of absorbers within the given layer. Consider nadir-view upwelling radiance for a given layer from z_0 to z_1 as an example. If no scattering occurs, and the temperature is constant within the layer, the upwelling radiance leaving the top boundary z_1 can be written as (Schwarzschild 1914)

$$\begin{aligned} I_{\nu}^{\uparrow}(z_1) &= I_{\nu}^{\uparrow}(z_0)e^{-[\tau_{\nu}(z_0)-\tau_{\nu}(z_1)]} + \int_{z_0}^{z_1} B_{\nu}[T(z)]\frac{d}{dz}e^{-[\tau_{\nu}(z)-\tau_{\nu}(z_1)]} dz \\ &= e^{-[\tau_{\nu}(z_0)-\tau_{\nu}(z_1)]}[I_{\nu}^{\uparrow}(z_0) - B_{\nu}(T)] + B_{\nu}(T), \end{aligned} \quad (1)$$

 Denotes content that is immediately available upon publication as open access.

Corresponding author: Chongxing Fan, cxfan@umich.edu

where ν denotes the frequency, $B_{\nu}(T)$ is the Planck function, and τ denotes the optical depth. The upwelling radiance at the top boundary is only related to three quantities, i.e., the upwelling radiance entering the lower boundary $I_{\nu}^{\uparrow}(z_0)$, the temperature of the layer, and the column concentration of the absorbers [related to $\tau(z_0) - \tau(z_1)$]. Suppose the entire atmospheric column is isothermal and the surface is a blackbody at the same temperature as the atmosphere. In that case, the first term on the right-hand side of Eq. (1) will be 0. The upwelling radiance at the top of the atmosphere will be simply the blackbody radiation of the surface temperature, regardless of how many absorbers are present in the atmosphere, i.e., no profiling capability for the atmosphere.

Given the well-known importance of thermal contrast in IR remote sensing, an interesting question to ask is, If scattering is presented in such an isothermal atmosphere, how much could it affect the above statement? Will it make an observable difference at the top of the atmosphere? In reality, clouds can have single scattering albedo as high as 0.85–0.9 in certain IR window or microwindow regions, e.g., ice cloud at the far-IR dirty window around 400 cm^{-1} and mid-IR window around 1100 cm^{-1} , and liquid clouds in the shortwave-IR window around 2700 cm^{-1} (Kuo et al. 2017). Even though, in reality, the entire atmosphere column cannot be isothermal, there are situations where the lower troposphere can be nearly isothermal. For example, the polar wintertime or the extrapolar regions during episodes of cold-air outbreaks tend to have nearly isothermal lower troposphere with persistent stratus clouds coverage at the same time. Thus, such a theoretical consideration of scattering in an isothermal atmosphere can be a good starting point to explore some real-world applications too.

The remaining sections are arranged as follows. Section 2 presents two-stream analytical solutions, as well as their

DOI: 10.1175/JAS-D-23-0050.1

© 2023 American Meteorological Society. This published article is licensed under the terms of the default AMS reuse license. For information regarding reuse of this content and general copyright information, consult the AMS Copyright Policy (www.ametsoc.org/PUBSReuseLicenses).

physical interpretations, to the scattering in an isothermal atmosphere for a variety of boundary conditions. Section 3 further illustrates the problem with a Monte Carlo approach and photon budget analysis. Section 4 quantifies the effect of scattering with a more sophisticated radiative transfer model with realistic molecular spectroscopy and cloud optical properties. Further discussion and speculations are presented in section 5.

2. Two-stream analytical solutions

As elegantly put by Bohren (1987), the two-stream approach, despite its simplicity, can provide many physical insights into multiple scattering problems. Here we use such an approach to illuminate the key physics behind the scattering in an isothermal, absorptive atmosphere. We start with the two-stream approximation following Fu et al. (1997). For a plane-parallel atmosphere, the upward and downward radiances measured at a certain atmospheric layer $d\tau$ in the thermal infrared can be correspondingly written as

$$\begin{aligned}\frac{\partial I^\uparrow}{\partial \tau} &= r_1 I^\uparrow - r_2 I^\downarrow - S, \\ \frac{\partial I^\downarrow}{\partial \tau} &= r_2 I^\uparrow - r_1 I^\downarrow + S,\end{aligned}\quad (2)$$

where

$$\begin{aligned}r_1 &= D \left[1 - \frac{\tilde{\omega}}{2} (1 + g) \right], \\ r_2 &= D \frac{\tilde{\omega}}{2} (1 - g), \\ S &= D(1 - \tilde{\omega})B[T(\tau)],\end{aligned}$$

τ is the optical depth, $D = 1.66$, $\tilde{\omega}$ is the single scattering albedo, g is the asymmetric factor. The Planck function $B[T(\tau)]$ depends on the temperature of that layer and is assumed to vary exponentially with τ [i.e., $B[T(\tau)] = ae^{\beta\tau}$, where $a = B_1$ and $\beta = (1/\tau_0)\ln(B_0/B_1)$]. In this definition, B_0 and B_1 are the Planck functions for the temperature at the bottom and top of a given layer, respectively, and τ_0 is the total optical thickness of this layer. All quantities are functions of frequency. For simplicity, the subscript ν is omitted. The general solution to Eq. (2) can be written as (Fu et al. 1997)

$$\begin{aligned}I^\uparrow(\tau) &= g_1 e^{-k(\tau_0 - \tau)} + g_2 Re^{-k\tau} + Z_+, \\ I^\downarrow(\tau) &= g_1 Re^{-k(\tau_0 - \tau)} + g_2 e^{-k\tau} + Z_-, \end{aligned}\quad (3)$$

where

$$\begin{aligned}k &= (r_1^2 - r_2^2)^{1/2}, \\ R &= \frac{r_1 - k}{r_2} = \frac{r_2}{r_1 + k}, \\ Z_\pm &= \frac{S}{k^2 - \beta^2} (r_1 \pm \beta + r_2),\end{aligned}$$

τ_0 is the total optical thickness from surface to TOA, and g_1 and g_2 are two constants to be determined by the boundary

conditions. Now if the atmosphere is isothermal, $\beta = 0$, $B_0 = B_1$, then

$$Z_+ = Z_- = \frac{D(1 - \tilde{\omega})B_0}{r_1 - r_2}. \quad (4)$$

From the definitions of r_1 and r_2 , it can be shown that

$$\begin{aligned}r_1 + r_2 &= D(1 - g\tilde{\omega}), \\ r_1 - r_2 &= D(1 - \tilde{\omega}).\end{aligned}\quad (5)$$

We can get

$$Z_+ = Z_- = B_0 = B_1. \quad (6)$$

The physical meaning of the Z_\pm terms is straightforward: they are the source term due to thermal emission in a given layer. We will then look at different sets of boundary conditions and explore the meanings of the solutions.

a. A trivial solution: Blackbody surfaces at both upper and lower boundaries

If the boundary conditions are

$$\begin{aligned}I^\uparrow(\tau_0) &= B_0, \\ I^\downarrow(0) &= B_0,\end{aligned}\quad (7)$$

i.e., both upper and lower boundaries can emit blackbody radiation at the same temperature as the isothermal layers, we have

$$\begin{aligned}g_1 + g_2 Re^{-k\tau_0} + Z_+ &= B_0, \\ g_1 Re^{-k\tau_0} + g_2 + Z_- &= B_0,\end{aligned}\quad (8)$$

which leads to $g_1 = g_2 = 0$, and $I^\uparrow(\tau) = I^\downarrow(\tau) = B_0$, i.e., the radiation fields are entirely constant, regardless of the actual values of $\tilde{\omega}$, g , and τ .

b. Blackbody bottom and space top

If the boundary conditions are

$$\begin{aligned}I^\uparrow(\tau_0) &= B_0, \\ I^\downarrow(0) &= 0,\end{aligned}\quad (9)$$

i.e., the underlying surface is blackbody and there is no downwelling flux at the top, then g_1 and g_2 can be solved as

$$\begin{aligned}g_1 &= \frac{Re^{-k\tau_0}Z_- - Z_+ + B_0}{1 - R^2e^{-2k\tau_0}} = B_0 \frac{Re^{-k\tau_0}}{1 - R^2e^{-2k\tau_0}}, \\ g_2 &= -\frac{Z_- - Z_+Re^{-k\tau_0} + B_0Re^{-k\tau_0}}{1 - R^2e^{-2k\tau_0}} = -B_0 \frac{1}{1 - R^2e^{-2k\tau_0}}.\end{aligned}\quad (10)$$

To illustrate the physics further, it is instructive to look at several extreme cases before we discuss the generic interpretation.

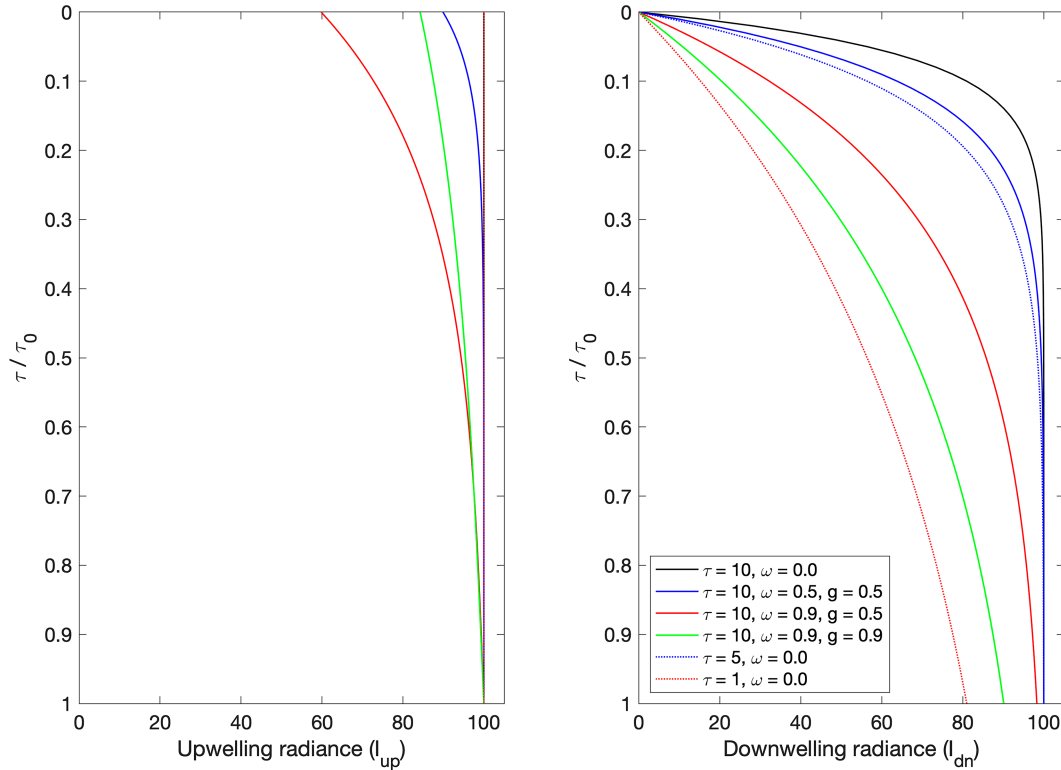


FIG. 1. The two-stream solution for an isothermal atmosphere with an underlying blackbody surface of the same temperature and zero downward radiance at the top of the atmosphere. The (left) upwelling and (right) downwelling radiances are shown. The blackbody radiation at the surface and atmospheric temperature is 100 (arbitrary unit). Results from different combinations of single scattering albedos and asymmetry factors are shown in different colors as labeled.

1) PURE ABSORPTION CASE ($\tilde{\omega} = 0$)

If $\tilde{\omega} = 0$, then $r_1 = D$ and $r_2 = 0$. Equation (10) leads to $g_1 = 0$ and $g_2 = -B_0$. Thus,

$$\begin{aligned} I^\uparrow(\tau) &= B_0, \\ I^\downarrow(\tau) &= B_0(1 - e^{-D\tau}). \end{aligned} \quad (11)$$

This is fully consistent with the formal solution without scattering, i.e., the upwelling radiance at any level is always blackbody radiation, and the downwelling radiance increases with the absorption optical depth of τ . Since the upwelling radiance is always constant without dependence on τ , there is no way to infer atmospheric profiles from the observation at the top of the atmosphere.

2) PURE FORWARDING SCATTERING ($g = 1$)

If $g = 1$ (i.e., all photons will be scattered forward instead of backward), we will have $r_1 = D(1 - \tilde{\omega})$ and $r_2 = 0$. The values of g_1 and g_2 are still the same as those in the case above (i.e., $g_1 = 0$ and $g_2 = -B_0$). As a result, we will get

$$\begin{aligned} I^\uparrow(\tau) &= B_0, \\ I^\downarrow(\tau) &= B_0[1 - e^{-D(1-\tilde{\omega})\tau}], \end{aligned} \quad (12)$$

which is the same as the results in section 2b(1) except that the absorption optical depth here is $(1 - \tilde{\omega})\tau$. Thus, if there is no backward scattering, the upwelling radiance is still just the blackbody radiation at any level.

3) SEMI-INFINITE ATMOSPHERE ($\tau_0 \rightarrow +\infty$)

The semi-infinite atmosphere implies $e^{-k\tau_0} = e^{-2k\tau_0} = 0$, which leads to $g_1 = 0$ and $g_2 = -B_0$. Thus,

$$\begin{aligned} I^\uparrow(\tau) &= B_0(1 - Re^{-k\tau}), \\ I^\downarrow(\tau) &= B_0(1 - e^{-k\tau}). \end{aligned} \quad (13)$$

At the top of the atmosphere, the upwelling radiance is no longer blackbody radiation. Instead, it is $B_0(1 - R)$, where R is associated with the scattering properties. Only at the level where $k\tau \gg 1$, the upwelling radiance approaches B_0 , so does the downwelling radiance.

4) GENERIC CASES

Figure 1 shows the solutions to several combinations of $\tilde{\omega}$ and g for an isothermal atmosphere with a total optical depth of 10. Compared to the pure absorption case (i.e., black line in Fig. 1), scattering reduces upwelling radiance at the TOA as long as backscattering exists, even though the atmosphere

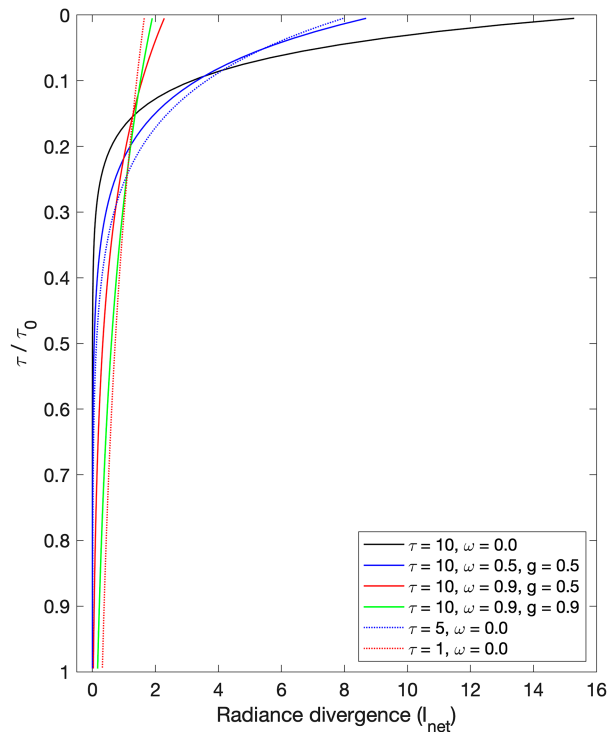


FIG. 2. The radiance divergence, i.e., $d(I^\uparrow - I^\downarrow)/d\tau$, for the same four solid line cases and two dashed line cases shown in Fig. 1.

is entirely isothermal. In the presence of scattering, the downwelling radiance is also reduced at all levels compared to the counterpart without scattering. Note the emissivity of each atmospheric layer, ε , is directly related to the absorptive optical thickness of the same layer ($\Delta\tau_{\text{abs}}$) by $\varepsilon = 1 - e^{-\Delta\tau_{\text{abs}}}$. Therefore, for the same extinction optical depth, the presence of scattering reduces the emissivity of each layer compared to the nonscattering case, i.e., the thermal emission of each layer is smaller, which contributed to such reduced downwelling radiance. Compared to the isothermal nonscattering cases in which the absorptive optical depth is the same (dash lines in the right panel of Fig. 1), the downwelling radiance is indeed increased at all levels in the presence of scattering. The radiance divergence (i.e., radiative cooling), as shown in Fig. 2, increases in the lower part of the atmosphere and decreases toward the TOA. As a result, in the presence of scattering, the increase of radiance cooling toward the TOA is not as sharp as in the nonscattering case. This is consistent with the fact that scattering is a diffusive process compared to pure absorption or emission.

Contrasting results between sections 2a and 2b, it is obvious that the boundary condition matters here for such deviation from blackbody behavior. In the real world, the lower troposphere can be close to isothermal in some weather conditions. Downwelling radiance at the upper boundary of such an isothermal layer is not zero, which is different from the idealized case above. However, scattering can still make a difference even if there is downwelling radiance at the upper boundary. The only exception is that the amount of downwelling radiance

across the upper boundary is the amount of radiance emitted by a surface with the same temperature as the isothermal-layer temperature [i.e., the boundary condition described by Eq. (7) in section 2a].

3. Monte Carlo simulation and photon “budget” analysis

To further understand the contribution of scattering to TOA radiances, we carried out a two-stream Monte Carlo simulation so the trajectory of each photon can be traced and counted. In the simulation, photons can be emitted from the surface as well as any layers within the atmosphere, and they travel in either upward or downward directions. When traveling through the atmosphere, each photon has a chance to interact with particles within a layer. The probability is dictated by the optical thickness of the layers. For those which interact with the atmosphere, they could be absorbed or scattered, forward or backward, as determined by single scattering albedo and asymmetry factor. We trace each photon to its destination and count the number of photons that get absorbed by each layer in the atmosphere, reach the surface, or reach the TOA, respectively. To be consistent with the two-stream analytical solution in the previous section, the zenith angle (μ) along the upward and downward direction is set at $\cos\mu = 1/1.66$. The number of photons released from the surface is 10^6 . The atmosphere is divided into 100 layers with equal optical thickness and the number of photons emitted from each layer depends on the emissivity of the layer (i.e., 10^6 photons are emitted if $\varepsilon = 1$). Compared to the theoretical derivation, the Monte Carlo method allows us to trace each photon and count the statistics. Table 1 shows such budget analyses for three cases in Figs. 1 and 2:

- Case 1: $\tau = 10$, $\tilde{\omega} = 0$ (black solid line in Figs. 1 and 2)
- Case 2: $\tau = 10$, $\tilde{\omega} = 0.5$, $g = 0.5$ (blue solid line in Figs. 1 and 2)
- Case 3: $\tau = 5$, $\tilde{\omega} = 0$ (blue dashed line in Figs. 1 and 2)

Cases 1 and 2 have the same extinction optical depth but case 1 has no scattering. Cases 2 and 3 have the same absorptive optical depth (thus the same number of photons emitted by the atmosphere) but case 3 has no scattering. The results from Monte Carlo simulations agree well with the analytical solutions, as shown in Fig. 3. The differences between them are within 0.25 units throughout the atmosphere (inset in each panel).

For the cases with the same extinction optical depth, total photons emitted by the atmosphere are reduced in the presence of scattering. As a result, although a higher percentage of atmospheric upward emission can reach the TOA in case 2 than in case 1 (10.4% vs 6.5%), case 1 still has more photons originating from the upward atmosphere emission and reaches the TOA than case 2 does. In case 2, only 0.9% of the total photons emitted downward are reflected to the TOA, which cannot change the contrast between case 1 and case 2.

For the cases with the same absorption optical depth, the number of photons emitted by the atmosphere is thus identical. Scattering in case 2 leads to $\sim 0.9\%$ of upward photons emitted by the atmosphere being removed by reflection to the

TABLE 1. Photon budget analysis based on two-stream Monte Carlo simulation for three opaque cases. Photons are traced and counted for their emission origins (surface, upward or downward from the atmosphere) and their final destinations (reaching TOA, absorbed by the surface, and absorbed by the atmosphere). Cases 1 and 2 have identical extinction optical depth and cases 2 and 3 have identical absorptive optical depth.

	Total number of emitted photons	Number of photons reaching the TOA	Number of photons absorbed by the surface	Number of photons absorbed within the atmosphere
Case 1: $\tau = 10$, $\tilde{\omega} = 0$				
Surface	1 000 000 (100%)	0 (0%)	0 (0%)	1 000 000 (100%)
Atmosphere (upward emission)	15 295 400 (100%)	999 534 (6.5%)	0 (0%)	14 295 866 (93.5%)
Atmosphere (downward emission)	15 295 400 (100%)	0 (0%)	998 790 (93.5%)	14 296 610 (6.5%)
Case 2: $\tau = 10$, $\tilde{\omega} = 0.5$, $g = 0.5$				
Surface	1 000 000 (100%)	46 (0.0%)	101 728 (10.2%)	898 226 (89.8%)
Atmosphere (upward emission)	7 964 900 (100%)	825 285 (10.4%)	75 145 (0.9%)	7 064 470 (88.7%)
Atmosphere (downward emission)	7 964 900 (100%)	75 818 (0.9%)	824 624 (10.4%)	7 064 458 (88.7%)
Case 3: $\tau = 5$, $\tilde{\omega} = 0$, $g = 0$				
Surface	1 000 000 (100%)	236 (0.0%)	0 (0%)	999 764 (100%)
Atmosphere (upward emission)	7 964 900 (100%)	999 581 (12.5%)	0 (0%)	6 965 319 (87.5%)
Atmosphere (downward emission)	7 964 900 (100%)	0 (0%)	1 000 213 (12.6%)	6 964 687 (87.4%)

surface, but it also puts the same number of downward photons emitted by the atmosphere reflected to the TOA. Meanwhile, scattering leads to more atmospheric absorption of photons (88.7% in case 2 vs 87.5% in case 3). As a result, the total number of photons reaching the TOA is less in case 2 than in case 3. For these cases, photons emitted from the surface have little chance of reaching the TOA due to the large optical depth. Case 2 shows 10% of surface emission reflected back to the surface due to scattering. Accordingly, there is a reduction in the number of photons reaching the TOA (or absorbed by the atmosphere) compared to case 3. If we let $g = 1$ in case 2, the photon budget will be identical to that of case 3 (no more than 0.1% difference in any category due to Monte Carlo sampling), consistent with the analytical solution discussed in section 2b(2).

Table 2 shows three sets of nonopaque cases. The budget analyses depicted above can be applied to such nonopaque cases as well. In a nutshell, for the cases with the same extinction optical depth, scattering implies less emission from the atmosphere, which leads to a reduction of the radiances that can reach the TOA. Reflection of surface emission back to the surface further contributes to the decrease of TOA upwelling radiances. For the cases with the same absorptive optical depth, backscattering contributes to the reduction of upwelling radiance at the TOA in two ways: 1) reducing the number of photons that are emitted from the surface and reach the TOA by the combined effect of atmospheric reflection and absorption; 2) reducing the number of photons emitted from the atmosphere and reach the TOA by increased atmospheric absorption (a consequence of scattering photons backward instead of forwarded). Note that, in this isothermal configuration, the reflection of atmospheric upward and downward emissions offset each other and make no contribution to the change of TOA upwelling radiance (as well as the change of surface downwelling radiance). As far as the TOA upwelling radiance is concerned, the real role of backward scattering is to increase the chance of photons being absorbed within the

atmosphere instead of reaching the boundaries (both top and bottom).

4. A more realistic simulation: 2016 East Asia cold wave

The above discussions are all based on highly idealized situations. To explore to what extent such isothermal scattering can affect the actual observations, we conduct more realistic simulations using actual sounding profiles of temperature and humidity and more sophisticated radiation transfer modeling, moderate resolution atmospheric transmission (MODTRAN) v5.2. MODTRAN is a radiative transfer code extensively used by the remote sensing community. Further details of it can be found in Anderson et al. (2007).

From 18 to 26 January 2016, East Asia was struck by a strong and broad cold-air outbreak. On 24 January, the Hong Kong Observatory at King's Park (WMO station ID 45004) recorded its coldest temperature in 59 years. The cold wave left Hong Kong blanketed by low clouds over days, with the lower troposphere nearly isothermal. Figure 4 shows the sounding profiles of temperature and dewpoint temperature reported by the King's Park station in Hong Kong at 1200 UTC 23 January 2016, as well as the true-color image, retrieved cloud optical thickness, and cloud-top pressure based on Aqua MODIS retrievals at 0600 UTC 23 January 2016, as summarized on NASA Worldview website (<https://worldview.earthdata.nasa.gov/>). It is clear from the temperature profile that the atmosphere is close to isothermal from the surface to ~ 3 km above. By using such a sounding profile, our primary goal in this section is to explore whether it is possible to detect water clouds within the isothermal layer from the TOA radiance, instead of developing a fully operational retrieval algorithm. Therefore, to produce simulated radiance as close as possible to the observed MODIS radiance is not a focus here, as many other factors besides cloud scattering can contribute to the differences between simulated and observed radiances.

In our MODTRAN calculation, cloud base is set at 1000 m, which is close to the lifting condensation level (LCL)

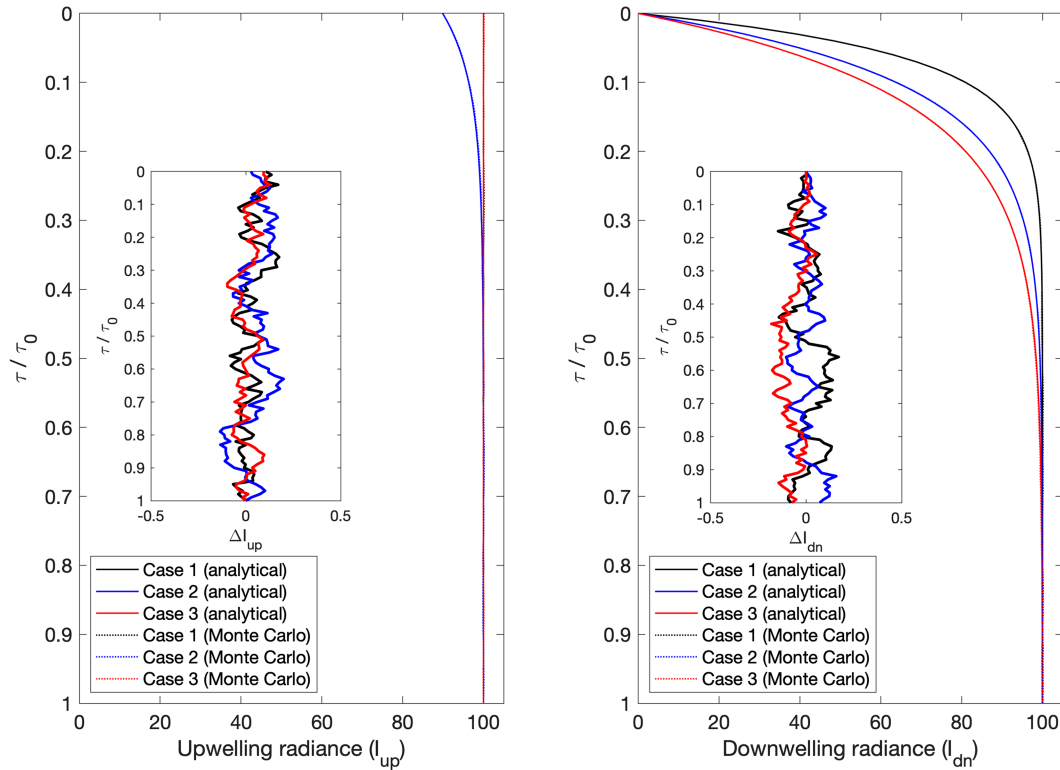


FIG. 3. The radiance fields for an isothermal atmosphere for the three cases investigated in Table 1. (left) Upwelling and (right) downwelling radiance are shown. The surface has the same temperature as the atmosphere, and its blackbody emission is 100 (arbitrary unit). Dash-dotted lines are results from a two-stream Monte Carlo simulation, and solid lines from the two-stream analytical solutions. They may not be visible since they overlap each other. The inset in each panel shows the radiance difference between the analytical and the Monte Carlo solutions.

decided by the sounding profile. Cloud top is determined to be ~ 600 hPa by the MODIS observations (Fig. 4). However, for the purpose of our study to study LW scattering in the isothermal layer and to avoid introducing the effect of scattering in a nonisothermal layer, the cloud top is deliberately set at 2000 m. MODIS-retrieved optical thickness is used as the cloud optical thickness in the calculation. All clouds here

are liquid clouds, and the default liquid cloud properties in MODTRAN are used. Four sets of MODTRAN calculations are conducted:

- 1) Clr noScat: Temperature and humidity profiles are based on the radiosonde observation. No clouds are specified in the model (i.e., clear sky). LW scattering is turned off.

TABLE 2. As in Table 1, but for three nonopaque cases.

	Total number of emitted photons	Number of photons reaching the TOA	Number of photons absorbed by the surface	Number of photons absorbed within the atmosphere
Case 1: $\tau = 2$, $\tilde{\omega} = 0$				
Surface	1 000 000 (100%)	36 711(3.7%)	0(0%)	963 289(96.3%)
Atmosphere (upward emission)	3 265 500 (100%)	963 925(29.5%)	0(0%)	2 301 575(70.5%)
Atmosphere (downward emission)	3 265 500 (100%)	0(0%)	963 846(29.5%)	2 301 654(70.5%)
Case 2: $\tau = 2$, $\tilde{\omega} = 0.5$, $g = 0.5$				
Surface	1 000 000 (100%)	129 463(12.9%)	99 549(10.0%)	770 988(77.1%)
Atmosphere (upward emission)	1 646 300(100%)	710 645(43.2%)	60 929(3.7%)	874 726(53.1%)
Atmosphere (downward emission)	1 646 300(100%)	60 677(3.7%)	709 839(43.1%)	875 784(53.2%)
Case 3: $\tau = 1$, $\tilde{\omega} = 0$, $g = 0$				
Surface	1 000 000(100%)	190 281(19.0%)	0(0%)	809 719(81%)
Atmosphere (upward emission)	1 646 300(100%)	809 878(49.2%)	0(0%)	836 422(50.8%)
Atmosphere (downward emission)	1 646 300(100%)	0(0%)	808 805(49.1%)	837 495(50.9%)

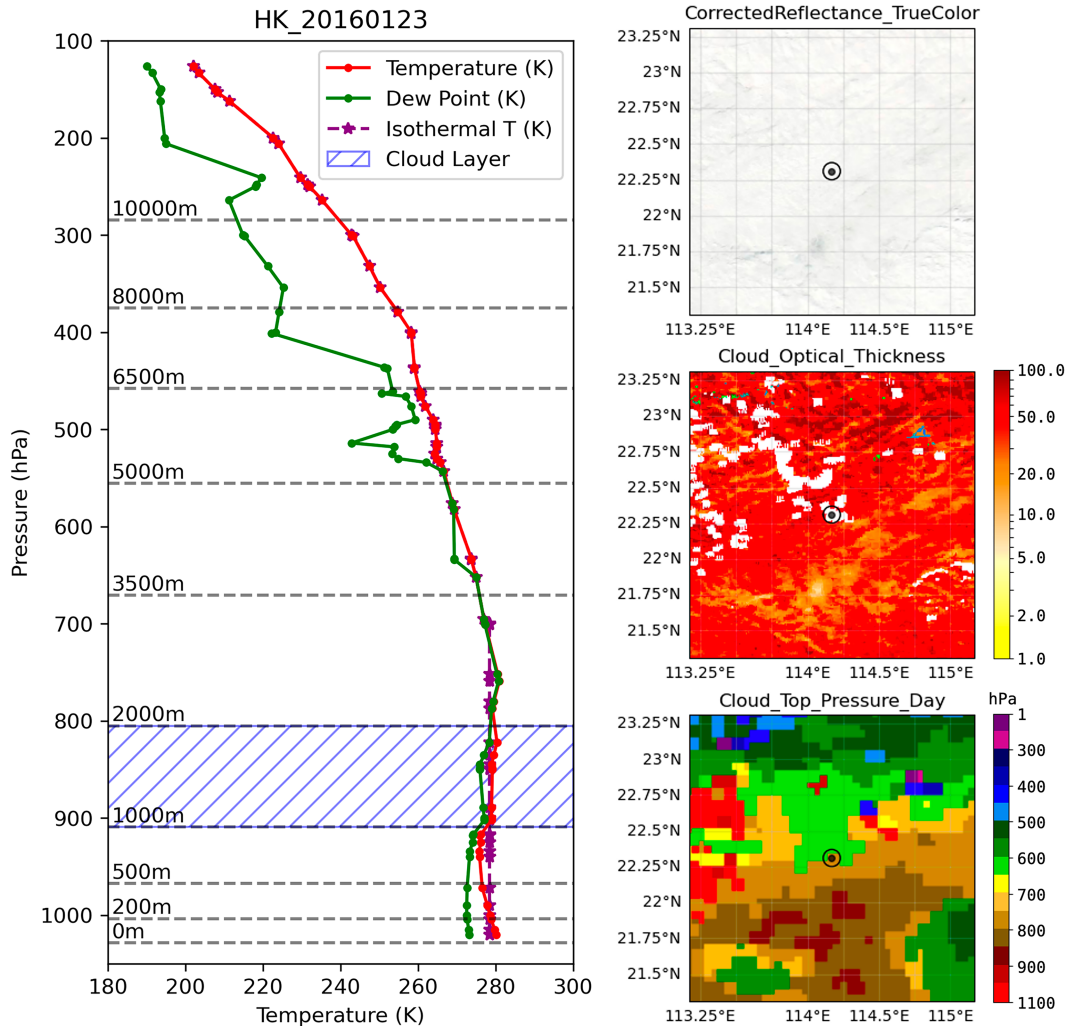


FIG. 4. (left) The sounding profile obtained at 1200 UTC 23 Jan 2016 by the Hong Kong Observatory: air temperature in red and dewpoint temperature in green. The blue hatched area indicates the cloud region set in the simulation. The purple line indicates the temperature profile assumed in cases 3 and 4, i.e., isothermal from the surface to 700 hPa and then identical to the actual sounding profile. (right) MODIS (top right) true color image, (middle right) retrieved cloud optical thickness, and (bottom right) cloud-top pressure derived from *Aqua* MODIS observation at 0600 UTC 23 Jan 2016. The location of the Hong Kong Observatory is labeled with a black circle with a square in its center. All right panels are produced using NASA Global Imagery Browse Services (GIBS).

- 2) Cld noScat: Same as 1, but a cloud is put in the isothermal layer (i.e., cloudy sky). It can only emit and absorb thermal IR radiation. The cloud properties are specified as described above.
- 3) Clr Scat: Same as 1, but LW scattering is enabled (essentially the same as case 1).
- 4) Cld Scat: Same as 2, but LW scattering is enabled. Clouds can now scatter thermal IR radiation.

The remaining configurations for all cases are the same. All greenhouse gases except water vapor are assumed at the default values of midlatitude winter prescribed in MODTRAN. Simulations are then carried out at 2-cm^{-1} spectral resolution (FWHM).

Cloud radiative effect on TOA radiance can be derived by subtracting TOA radiance in cloudy-sky cases from that in clear-sky cases (i.e., case 2 – case 1 and case 4 – case 3). Figure 5a shows the simulated cloud radiative effect on TOA radiance when LW scattering is enabled (red line) or disabled (blue line). As discussed in previous sections, in the absence of LW scattering, upwelling radiance at the top of an isothermal layer is independent of the amount of absorption within that layer. Because the temperature profile in the real world is not perfectly isothermal, adding an absorbing cloud within the quasi-isothermal layer will result in a small difference in simulated TOA radiance (blue line). However, when LW scattering is included in the simulation, there is a large dip at the atmospheric window region (red line), indicating that the

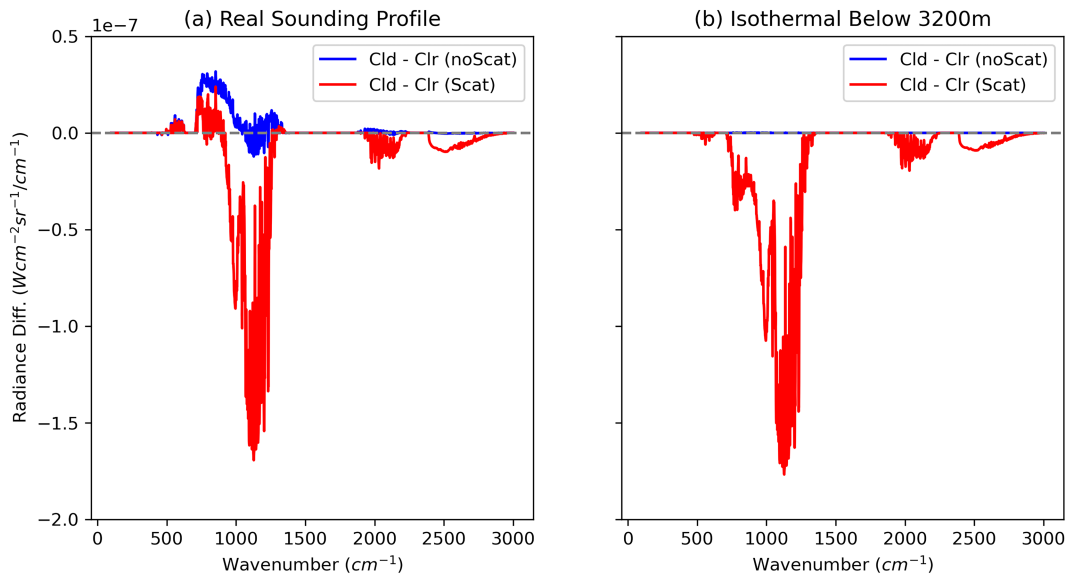


FIG. 5. (a) Simulated TOA radiance difference between the cloudy-sky case and the clear-sky case when LW scattering is enabled (red) or disabled (blue) using the real sounding profile at Hong Kong site at 1200 UTC 23 Jan 2016. (b) As in (a), except that the temperature from the surface to 3200 m is homogenized to create a perfect isothermal layer.

TOA radiance is reduced because of the added cloud layer. Figure 5b shows a case where the atmospheric temperature from surface to 3200 m is set constant. The blue line is now completely flat at zero, suggesting that the added cloud layer will make no impact on TOA radiance when cloud LW scattering is ignored. When the LW scattering physics is included, however, a difference in TOA radiance can be clearly seen (red line in Fig. 5b), with similar magnitude in the window region as its counterpart in Fig. 5a.

To see how our results can be applied in remote sensing problems, we convolved simulated radiance with the spectral response functions of MODIS channels 28–31, i.e., channels in the mid-IR window and at the edge of the H₂O band, to produce nadir-view synthetic MODIS radiances. Figure 6 shows the differences in simulated brightness temperature (BT) due to clouds in the nearly isothermal layer at MODIS IR channels 27–36. To show the capability to retrieve cloud properties, we added two cases where cloud optical thickness is different. When LW scattering is ignored (Fig. 6a), the change in BT is within 0.25 K throughout the MODIS IR channels. The LW scattering in the nearly isothermal layer can cause a much larger BT difference, especially at MODIS band 29 (Fig. 6b). The BT dip at MODIS band 29 is approximately 1.25 K when cloud optical thickness is large ($\tau_{\text{vis}} = 10$ and 60) and nearly 0.75 K when cloud optical thickness is small ($\tau_{\text{vis}} = 1$). The BT decrease at MODIS band 30 is ~ 0.5 K for all cases. The BT difference at other MODIS IR bands is much smaller. We also calculated the BT differences when the atmospheric temperature from surface to 3200 m is set to be constant. Figures 6c and 6d show that when a cloud is added to an isothermal layer, it is impossible to detect it based on TOA radiance without scattering being included. Only when LW

scattering is included in our simulation can we see a reduced brightness temperature at MODIS bands 29–32. The amount of decrease depends on cloud properties such as cloud optical thickness (Fig. 6d). Such dependency enables us to retrieve cloud properties in this isothermal layer from the space.

5. Conclusions and discussion

Using an analytical two-stream solution and a Monte Carlo approach, we examine how the thermal IR scattering can affect the radiation field under a special circumstance, i.e., an isothermal atmosphere. Without scattering, the radiation field for an isothermal atmosphere with an underneath blackbody surface can be easily understood using Kirchhoff's law: the upwelling radiance always follows the blackbody radiation regarding the actual values of optical properties in any atmospheric layer, and the downwelling radiance increases with the optical depth. With scattering, however, the upwelling radiance no longer follows Planck's law. Instead, as long as the asymmetry factor is less than one, the TOA upwelling radiance will be smaller than the blackbody radiation. Compared to a nonscattering isothermal atmosphere with the same extinction optical depth, the presence of scattering implies a smaller absorption optical depth and, consequently, leads to a smaller emissivity (i.e., a larger transmissivity) for the atmosphere. This further leads to two opposite effects: a reduction of the total amount of atmospheric thermal emission and an increase in the amount of surface emission that can reach the TOA. The first effect outweighs the latter one and leads to a reduction of upwelling radiance at the TOA (note two effects would perfectly cancel each other if no scattering were presented and only a reduction of optical depth happened). Compared to a nonscattering isothermal atmosphere with the

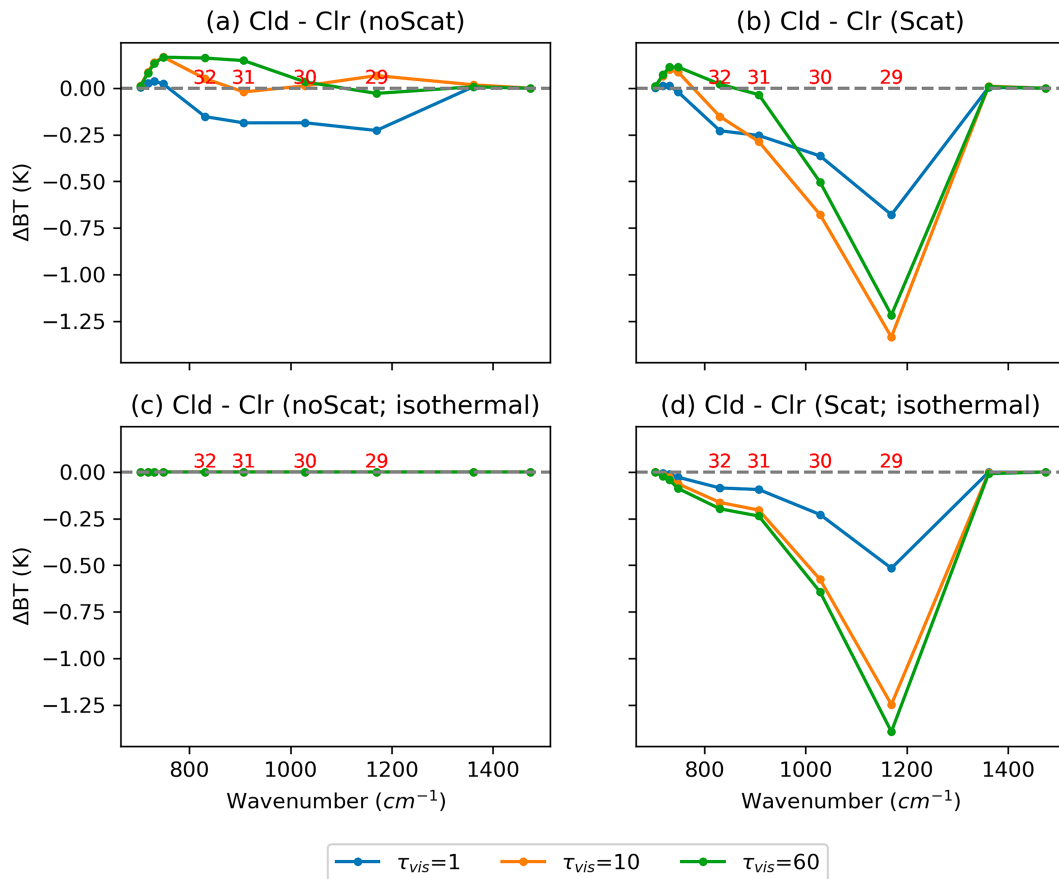


FIG. 6. Changes of the simulated brightness temperatures (BTs) over MODIS IR channels when a cloud layer is added to the nearly isothermal layer. (a) LW scattering is not included; (b) LW scattering is included; (c),(d) as in (a) and (b), except the atmospheric temperature in the nearly isothermal layer is set to be constant so that it becomes perfectly isothermal. MODIS bands 29–32 are labeled using red font. Different colors represent different visible optical thickness of the cloud layer.

same *absorption* optical depth, backscattering increases the chance of photons (regardless of their origin) being absorbed within the atmosphere instead of reaching the boundaries (both top and bottom). Consequently, the TOA upwelling radiance also becomes smaller than the blackbody radiation. Using sounding profiles and more realistic and sophisticated radiative transfer modeling, we further show that such scattering effect of isothermal cloud can cause approximately -1.5-K brightness temperature difference for the nadir-view radiance of MODIS channel 29, a mid-IR window channel frequently used for cloud retrievals.

Thermal contrast (i.e., temperature gradient) is a prerequisite for infrared remote sensing in absence of scattering. However, we showed here that even in the absence of thermal contrast, scattering could affect the TOA radiance. Thus, it allows one to infer cloud properties with such scattering signals even when thermal contrast does not exist. Here we use an actual sounding profile in the subtropics under a severe cold-air outbreak event to illustrate how the cloud scattering within a nearly isothermal layer can affect the TOA radiance. Liquid cloud is used in our study. A nearly isothermal layer

can be encountered in polar regions, where the clouds could be mixed phased or ice. Ice clouds have similar single scattering albedo and asymmetric factor as liquid clouds in the mid-IR window region and higher single scatter albedo in the far-IR dirty window (Kuo et al. 2017). Therefore, the same LW scattering mechanism could also be useful for polar cloud observations. Furthermore, scattering affects not only the scalar radiance field but also the polarization of the radiation (Coy et al. 2020; Shanks 2022). Thus, it can be expected that polarized IR measurements can further enhance cloud retrieval capability under such isothermal environments.

Acknowledgments. We sincerely acknowledge three anonymous reviewers for their insightful suggestions on improving the quality and clarity of our article. XLH thanks Graeme Stephens for inspirational discussions, which partly motivated this study. Lead author CXF is supported by the NASA FINNIST program under Grant 80NSSC22K1433. Part of XLH's effort is supported by NOAA Grant NA20NES4400007 with a subcontract from Texas A&M University.

Data availability statement. We acknowledge the use of MODIS images and retrievals provided by services from NASA's Global Imagery Browse Services (GIBS), part of NASA's Earth Observing System Data and Information System (EOSDIS). They can be accessed at <https://gibs.earthdata.nasa.gov/>. The sounding data can be downloaded from the Department of Atmospheric Science at University of Wyoming (<https://weather.uwyo.edu/upperair/sounding.html>). MODTRAN is a radiative transfer simulation software that can be purchased from Spectral Sciences Inc. (<http://modtran.spectral.com/>).

REFERENCES

- Anderson, G. P., and Coauthors, 2007: Using the MODTRAN5 radiative transfer algorithm with NASA satellite data: AIRS and SORCE. *Proc. SPIE*, **6565**, 65651O, <https://doi.org/10.1117/12.721184>.
- Bohren, C. F., 1987: Multiple scattering of light and some of its observable consequences. *Amer. J. Phys.*, **55**, 524–533, <https://doi.org/10.1119/1.15109>.
- Chahine, M. T., 1974: Remote sounding of cloudy atmospheres. I. The single cloud layer. *J. Atmos. Sci.*, **31**, 233–243, [https://doi.org/10.1175/1520-0469\(1974\)031<0233:RSOCAI>2.0.CO;2](https://doi.org/10.1175/1520-0469(1974)031<0233:RSOCAI>2.0.CO;2).
- Coy, J. J., A. Bell, P. Yang, and D. L. Wu, 2020: Sensitivity analyses for the retrievals of ice cloud properties from radiometric and polarimetric measurements in sub-mm/mm and infrared bands. *J. Geophys. Res. Atmos.*, **125**, e2019JD031422, <https://doi.org/10.1029/2019JD031422>.
- Fu, Q., K. N. Liou, M. C. Cribb, T. P. Charlock, and A. Grossman, 1997: Multiple scattering parameterization in thermal infrared radiative transfer. *J. Atmos. Sci.*, **54**, 2799–2812, [https://doi.org/10.1175/1520-0469\(1997\)054<2799:MSPITI>2.0.CO;2](https://doi.org/10.1175/1520-0469(1997)054<2799:MSPITI>2.0.CO;2).
- Inoue, T., 1985: On the temperature and effective emissivity determination of semi-transparent cirrus clouds by bi-spectral measurements in the 10 μ m window region. *J. Meteor. Soc. Japan*, **63**, 88–99, https://doi.org/10.2151/jmsj1965.63.1_88.
- Kaplan, L. D., 1959: Inference of atmospheric structure from remote radiation measurements. *J. Opt. Soc. Amer.*, **49**, 1004–1007, <https://doi.org/10.1364/JOSA.49.001004>.
- Kuo, C.-P., P. Yang, X. Huang, D. Feldman, M. Flanner, C. Kuo, and E. J. Mlawer, 2017: Impact of multiple scattering on long-wave radiative transfer involving clouds. *J. Adv. Model. Earth Syst.*, **9**, 3082–3098, <https://doi.org/10.1002/2017MS001117>.
- McCleese, D. J., and L. S. Wilson, 1976: Cloud top heights from temperature sounding instruments. *Quart. J. Roy. Meteor. Soc.*, **102**, 781–790, <https://doi.org/10.1002/qj.49710243408>.
- McMillin, L. M., 1975: Estimation of sea surface temperatures from two infrared window measurements with different absorption. *J. Geophys. Res.*, **80**, 5113–5117, <https://doi.org/10.1029/JC080i036p05113>.
- Schwarzschild, K., 1914: Diffusion and absorption in the sun's atmosphere. *Sitzungsberichte der Königlich Preussischen Akademie der Wissenschaften*, 1183–1200.
- Shanks, K. A., 2022: Infrared polarimetry for remote sensing. Ph.D. dissertation, James C. Wyant College of Optical Sciences, The University of Arizona, 170 pp., <http://hdl.handle.net/10150/664364>.
- Smith, W. L., H. M. Woolf, and W. J. Jacob, 1970: A regression method for obtaining real-time temperature and geopotential height profiles from satellite spectrometer measurements and its application to Nimbus 3 "SIRS" observations. *Mon. Wea. Rev.*, **98**, 582–603, [https://doi.org/10.1175/1520-0493\(1970\)098<0582:ARMFOR>2.3.CO;2](https://doi.org/10.1175/1520-0493(1970)098<0582:ARMFOR>2.3.CO;2).
- Wang, C., S. Platnick, Z. Zhang, K. Meyer, and P. Yang, 2016a: Retrieval of ice cloud properties using an optimal estimation algorithm and MODIS infrared observations: 1. Forward model, error analysis, and information content. *J. Geophys. Res. Atmos.*, **121**, 5809–5826, <https://doi.org/10.1002/2015JD024526>.
- , —, —, —, G. Wind, and P. Yang, 2016b: Retrieval of ice cloud properties using an optimal estimation algorithm and MODIS infrared observations: 2. Retrieval evaluation. *J. Geophys. Res. Atmos.*, **121**, 5827–5845, <https://doi.org/10.1002/2015JD024528>.